Editors' Suggestion

Time-resolved measurement of spin excitations in Cu_2OSeO_3

D. M. Burn,[1] S. L. Zhang,[2,3] G. van der Laan,[1] and T. Hesjedal[4]
[1]*Diamond Light Source, Harwell Science and Innovation Campus, Didcot OX11 0DE, United Kingdom*
[2]*School of Physical Science and Technology, ShanghaiTech University, Shanghai 200031, China*
[3]*ShanghaiTech Laboratory for Topological Physics, ShanghaiTech University, Shanghai 200031, China*
[4]*Clarendon Laboratory, Department of Physics, University of Oxford, Parks Road, Oxford OX1 3PU, United Kingdom*

(Received 6 September 2022; accepted 28 October 2022; published 9 November 2022)

Magnetic diffraction in combination with x-ray detected ferromagnetic resonance (DFMR) is a powerful technique for performing time-resolved measurements on individual spin textures. Here, we study the ferromagnetic resonance (FMR) modes of both the conical and field-polarized phases in the chiral magnet Cu_2OSeO_3. Following the identification of the FMR modes at different temperatures using broadband vector network analyzer FMR, we use DFMR on the crystalline (001) Bragg peak to reveal the time-dependent spin configurations of the selected FMR modes. By being able to measure both the amplitude and phase response of the spin system across the resonance, a continuous phase advance (of 180°) in the conical mode and a phase lag (of 180°) in the field-polarized mode is found. By performing dynamic measurements in the conical phase as a function of the linear polarization angle of the x rays, i.e., successively probing the dynamics of the moments, we find an inversion of the dynamics along the conical axis upon inverting the applied field direction. By allowing for time-resolved measurements of the phase and amplitude of individual magnetic phases, DFMR opens up new opportunities for obtaining a deeper understanding of the complex dynamics of chiral magnets.

DOI: 10.1103/PhysRevB.106.174409

I. INTRODUCTION

Topological spin textures in chiral magnets such as Cu_2OSeO_3 are of great interest for potential advances in spintronics [1,2]. Key to the success of future technologies are their dynamic properties, enabling fast and energy-efficient transitions of the magnetic states. One of the most commonly used techniques for the study of the magnetization dynamics is ferromagnetic resonance (FMR) [3–6]. In broadband coplanar waveguide (CPW) FMR, the resonances of a sample are probed by placing it on the CPW and subjecting it to a variable magnetic field. By sweeping an rf signal fed to the CPW in a range from typically 0 to 20 GHz and by measuring the transmitted rf power, the resonances reveal themselves as absorption maxima in frequency vs field maps.

Previous vector network analyzer (VNA) FMR studies have probed the magnetization dynamics of the resonance modes in Cu_2OSeO_3, i.e., the helical, conical, and skyrmion phases, as well as the field-polarized phase, revealing their evolution in field-frequency space [1,7–10]. Supported by micromagnetic simulations, three internal breathing and rotational modes have been identified in the skyrmion phase [1], two each in the helical and conical states, and one in the field-polarized state [7].

Within the conical phase, the two resonance modes that have been resolved can be attributed to vibrational modes in the conical structure and are labeled $+Q$ and $-Q$ [1]. While their magnetization oscillates uniformly, the two modes have opposite helicities and oscillate (counter)clockwise in the $(+Q)$ $-Q$ mode [10]. For their excitation, the AC field has to be perpendicular to the bias field direction and hence the conical propagation axis [1]. In addition to the geometry of the field direction, the excitation also depends on the sample geometry due to the anisotropy [7,8]. The Gilbert damping parameter is small and was found to be <0.003 in Cu_2OSeO_3 at 5 K (from the FMR linewidth) [9]. Note that the counterclockwise oscillating $+Q$ mode seamlessly connects to the also counterclockwise oscillating Kittel mode present in the field-polarized phase above a critical field, while the spectral weight of the $-Q$ mode is vanishing. The counterclockwise rotation sense in the field-polarized state is a result of the fact that single-electron moments, representative of a uniform magnetic state, simply precess counterclockwise around a magnetic field vector.

Resonant elastic x-ray scattering (REXS) provides a unique, element-specific view of ordered magnetic structures and has been extensively used for the study of Cu_2OSeO_3 [11–15] and other chiral magnetic systems [16–21]. The use of soft x rays (via x-ray magnetic circular dichroism) to measure magnetization dynamics through x-ray detected ferromagnetic resonance (XFMR) is a valuable technique [22–25], giving access to the dynamics of individual layers via the element selectivity of x-ray spectroscopy in few-layer stacks such as spin valves [26] and magnetic tunnel junctions [27]. The combination of the two, REXS and XFMR, allows for dynamic studies of diffraction-selected specific magnetic modes and is particularly useful for systems in which the eigenmodes are complex and their interpretation crucially relies on micromagnetic simulations. The capabilities of this diffractive FMR (DFMR) technique were demonstrated on

the rich magnetic structure of a Y-type hexaferrite [28], and it was further expanded into the probing of superlattices via x-ray reflectometry [29]. A similar technique, REXS-FMR, was successfully applied for the study of, most notably, the three skyrmion eigenmodes in Cu_2OSeO_3 via the crystalline (001) Bragg peak and its magnetic satellites [30]. While REXS-FMR is a homodyne detection technique which relies on the difference of probed magnetic peak intensities between rf being on and off, heterodyne detection DFMR is a truly time-resolving technique, giving access to the phase of the dynamic response [28]. Also note that both REXS-FMR and DFMR can be carried out on the magnetic satellites as well; however, due to the complexity of the analysis, the present study will focus on dynamic Bragg peak studies.

Here, we report a time-resolved dynamic study of the conical and field-polarized phase in Cu_2OSeO_3 using the diffractive ferromagnetic resonance technique, employing both circularly and linearly polarized x rays. First, the dynamic phase diagram is mapped out using VNA-FMR with the field applied in plane, identifying the conical and field-polarized modes and characterizing their temperature and field dependence. The characteristics of the resonance modes in the conical and field-polarized phases, as well as the dependence of the critical field on temperature, are well captured using the established models [10]. Using DFMR, we investigate the dynamic behavior of the conical $+Q$ and the field-polarized mode, as well as the transition between them, in greater detail. As the field-polarized phase does not result in magnetic scattering peaks, we restrict our study to the analysis of the (001) Bragg peak, whose magnetic intensity is susceptible to both phases. Note that, in principle, any reflection peak which has a magnetic contribution could be probed. We find 180° phase shifts across the resonances of the conical and field-polarized modes, which are negative and positive, respectively. Further, while the conical resonance peak position is temperature dependent, the field-polarized resonance is temperature independent. Finally, by employing linear polarized x rays with a variable polarization angle, we are able to access the dynamics of the projected moments along the conical texture at resonance. We find that upon reversing the applied field, the dynamic response is inverted.

II. EXPERIMENT

The dynamic behavior of the conical and field-polarized phases in Cu_2OSeO_3 was measured using broadband VNA-FMR [31] and synchrotron-based DFMR [28]. Both techniques were performed *in situ* in the RASOR diffractometer on beamline I10 at the Diamond Light Source (Oxfordshire, United Kingdom). A high-quality, (001)-cut Cu_2OSeO_3 sample, measuring $2 \times 2 \times 0.1$ mm^3, was polished and placed on a CPW. The CPW was attached to a cold-finger cryostat at the center of the diffractometer and cooled to temperatures in the range from 25 to 60 K in ultrahigh vacuum. A magnetic bias field was applied in the plane of the sample by way of two permanent magnets, whereby the field strength can be controlled by varying the separation between the magnets. This bias field was oriented in the scattering plane and perpendicular to the rf field produced by the CPW. The schematic of the experimental setup is illustrated in Fig. 1.

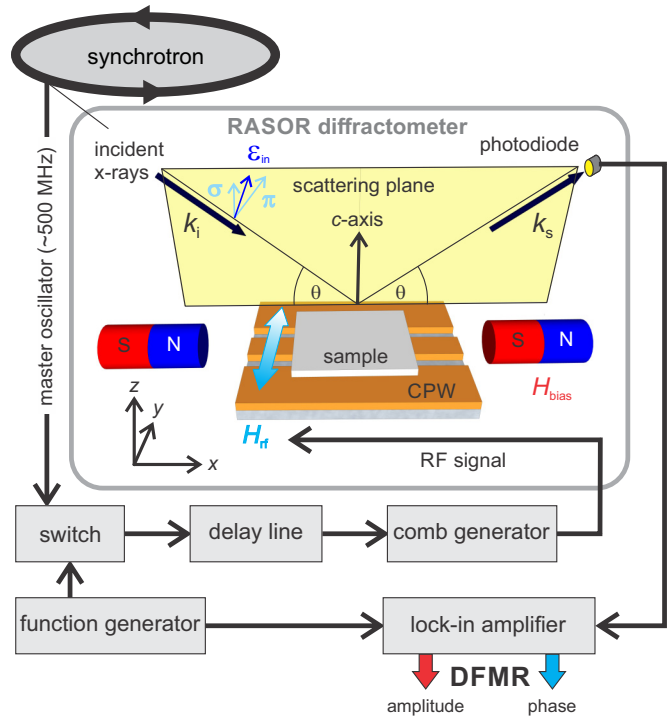

FIG. 1. Schematic of the ferromagnetic resonance setup, allowing for both VNA-FMR and DFMR measurements in the RASOR diffractometer at the Diamond Light Source. The Cu_2OSeO_3 sample is placed on the CPW, which is mounted on the cold finger inside the diffractometer. The incident x rays, which are tuned to the Cu L_3 edge, are scattered off the sample and detected via a photodiode in a θ-2θ geometry. Circularly as well as linearly polarized x rays were used, where the linear polarization ϵ_i was continuously variable, covering ϵ being in the scattering plane (π) and perpendicular to it (σ). A linear polarization angle of 0° corresponds to linear horizontal σ polarization. The variable magnetic field is applied in the scattering plane via pairs of permanent magnets whose distance can be controlled. An rf signal is fed to the CPW to drive the ferromagnetic resonance in the magnetic sample, with its field effectively being perpendicular to the scattering plane at the probed sample position. As the synchrotron gives x-ray pulses at a frequency of ∼500 MHz, a comb generator is used to produce higher harmonics, which are selected and fed to the CPW. To probe the time dependence of the scattered x-ray intensity, a tunable delay line is used, which shifts the phase between the pump (the rf signal) and the probe (the pulsed x rays).

First, the static magnetic scattering from the sample was characterized. Cu_2OSeO_3 [cubic space group $P2_13$ (no. 198)] has a lattice constant of 8.925 Å. At the Cu L_3 edge (931.25 eV), this results in the (001) structural Bragg peak at $2\theta = 96.5°$ [13]. Note that this (001) Bragg peak is "forbidden" and observed only in resonant x ray scattering [11,12,32,33]. In resonant scattering, the magnetic state of Cu_2OSeO_3 can be accessed via the structural Bragg peak [30]; that is, it effectively probes the $k = 0$ dynamics or, alternatively, the magnetic satellites ($k \neq 0$ modes, e.g., the skyrmion breathing mode) [11,12].

To cover an extended field range, the measurements were performed in two parts, where the smaller permanent magnets were replaced by larger ones for the second part of

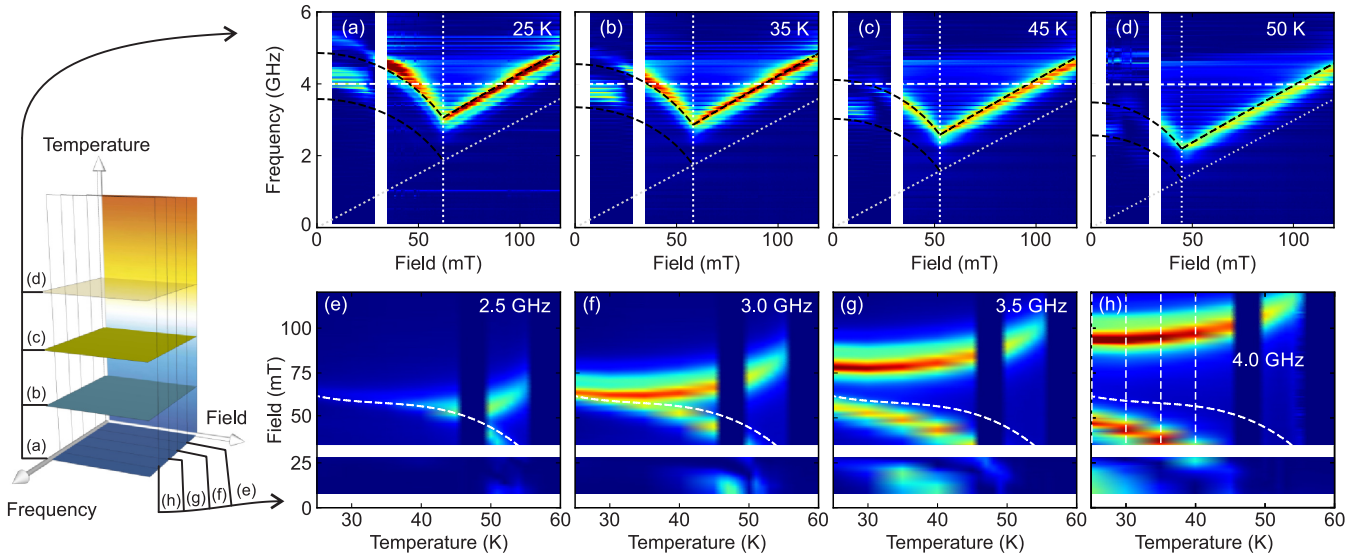

FIG. 2. Vector network analyzer ferromagnetic resonance measurements showing plots of the FMR spectra ΔS_{21} (linear scale in arbitrary units) for different measurement conditions. The data were obtained from a series of field-cooling temperature sweeps at different fields, with the field applied perpendicular to the rf excitation direction. Slices of the data show the absorption as a function of (a)–(d) frequency and field and (e)–(h) field and temperature. The strong absorption features represent magnetic resonance modes in the sample. The vertical dashed lines in (a)–(d) and curved lines in (e)–(h) represent the magnetic phase transition field H_{c2} between the conical and field polarized phases. Model plots of the resonance curves for both phases (black dashed lines) are overlaid on top of the data in (a)–(d), and the dotted white diagonal lines represent the behavior of the Kittel mode in a perfect sphere. The horizontal dashed lines at 4 GHz in (a)–(d) and the vertical dashed lines at 25, 30, 35, and 40 K in (h) indicate the parameters for which the DFMR measurements were carried out.

the measurements. As their field ranges were not perfectly overlapping, fields around 30 mT could not be covered (white regions in the resonance plots in Fig. 2).

As a first step, the dynamic phase space of the system was mapped out using VNA-FMR. The rf power transmitted through the CPW S_{21} is measured, where its loss ΔS_{21} as a function of frequency represents the FMR spectrum. In VNA-FMR measurements, this absorption is typically mapped out as a function of rf frequency and magnetic bias field. However, in this investigation, the absorbed rf power also depends on the magnetic phase of the sample and thus the excitable magnetic spin configurations, resulting in a temperature and extra field dependence of the spectra. Therefore, in this investigation, we map out the rf absorption of the sample as a function of all three quantities, i.e., frequency, field, and temperature. In practice, this is best achieved by performing frequency sweeps while slowly decreasing the temperature. The difference in sweep rates of both quantities means that the temperature deviation over the time taken to measure a frequency sweep is negligible. These measurements are then repeated at various magnetic fields. This effectively measures the dynamic properties of the system as prepared using a field-cooling protocol.

As the temperature was varied continuously while taking frequency sweeps, the temperature steps need to be interpolated to enable further processing and the analysis of two-dimensional slices of the frequency field at fixed temperature or field temperature at fixed frequency. In VNA-FMR measurements, the background resulting from the electrical characteristics of the measurement setup is subtracted. This background is typically obtained from a high-field measurement where the moments are saturated and any dynamic features are driven to sufficiently high frequencies to be out of the measurement range. Due to the limitations in the field range in the RASOR diffractometer, we adopt an alternative approach by subtracting a background measured in the field-polarized state at 60 K, i.e., at a temperature above T_C.

After the detection of the dynamic modes using VNA-FMR, the modes were further investigated using polarized soft x rays. Both circularly and linearly polarized x rays were used, with an energy tuned to the Cu L_3 edge at 931.25 eV. The beam spot size at the sample position is typically $100 \times 100\ \mu m^2$, and the scattered beam was measured using a photodiode in a θ-2θ configuration with slits providing an angular resolution of $\sim$3 mrad.

Initially, measurements of the scattered intensity as a function of reciprocal lattice space coordinates were used to map out the static magnetic phase diagram of the sample and to optimize the alignment of the diffractometer. The detector was then positioned at the (001) Bragg peak of Cu_2OSeO_3.

The polarized soft x rays provide a probe of the magnetization state in the sample due to circular and linear magnetic dichroism in resonant elastic x-ray scattering [34]. As noted above, in resonant scattering on Cu_2OSeO_3, both the (001) Bragg peak [30] and its surrounding magnetic satellites [11,12] can be used to probe the magnetic states of Cu_2OSeO_3. Here, due to the complexity of the depth-dependent information that a resonant soft x-ray study of the magnetic satellites provides, we focus on the analysis of the (001) Bragg peak data.

For the dynamic measurements, the scattered intensity at the (001) Bragg peak was measured stroboscopically, taking advantage of the pulsed nature of the synchrotron radiation at a frequency of $\sim$500 MHz. Here, the rf magnetic field generated by the CPW beneath the sample was phase locked

to an integer multiple of the synchrotron master clock. Due to the reduced thickness of the sample (∼100 μm), the rf power delivered from the CPW was sufficient to excite the magnetization precession dynamics on the Cu_2OSeO_3 top surface region probed by the x rays. The intensity of the scattered x rays provides a measure of the magnetic state of the system for a particular point in time during the precession of the magnetization. Taking such snapshots for increasing delay time between the rf pump and the x-ray probe then gives the time-dependent magnetization behavior. The signal-to-noise ratio in the dynamic component of the scattered intensity is further enhanced through lock-in detection, using a 180° modulation of the phase of the rf pump at a frequency of 700 Hz. For our measurements, the rf frequency was set to 4 GHz, where a clear FMR mode crossing is found for both the conical and field-polarized phases. Both of these mode crossings are within the field range accessible in the diffractometer. Measurements of the dynamic signal as a function of pump-probe delay and magnetic field were performed at various temperatures with both left and right circularly polarized x rays and also with linearly polarized x rays as a function of the incident polarization angle.

III. RESULTS

The ferromagnetic resonance modes of the Cu_2OSeO_3 sample were first studied in the RASOR diffractometer using VNA-FMR. The frequency spectra were measured during a series of field-cooling sweeps, i.e., as a function of temperature. Slices of these data as a function of frequency and field at different temperatures and also as a function of field and temperature at different frequencies are shown in Figs. 2(a)–2(d) and 2(e)–2(h), respectively. The color scale represents the magnitude of transmitted rf power ΔS_{21}, revealing strong absorption features corresponding to magnetic resonance modes in the sample.

At the critical field H_{c2}, an abrupt change in the magnetic resonance behavior is observed, which is indicated in Figs. 2(a)–2(d) by the vertical dashed lines and in Figs. 2(e)–2(h) by the curved dashed lines. This phase boundary separates the conical phase at lower fields from the field-polarized phase which exists above the transition. These phases show different magnetic resonance behaviors, and there is a continuous transition between them crossing the phase boundary.

The resonance behavior of the field-polarized mode above H_{c2} is adequately described by the Kittel equation, i.e., the description for a uniform ferromagnet (see Eq. (14) in Ref. [10]). Note that while the sample in the present case is a flat plate with its surface normal along the z direction (i.e., with demagnetization factors of $N_x \approx N_y \approx 0$ and $N_z \approx 1$), the static magnetic field is applied along the x direction, while the rf field H_{rf} is applied along the y direction (see Fig. 1). The measured resonance curves [Figs. 2(a)–2(d)] lie above the straight (white dotted) frequency-field line representing the behavior of a perfect sphere, i.e., when demagnetization is irrelevant (demagnetization factors $N_x = N_y = N_z = 1/3$) and $\hbar\omega = g\mu_{\mathrm{B}}\mu_0 H$, which is the resonance frequency in the paramagnetic limit. Note that the field-polarized phase branch can lie either above (as here) or below the paramagnetic resonance (dotted white lines), depending on whether the shape anisotropy effectively enhances or reduces the applied static field [35].

From fitting the Kittel equation to the data [dashed black lines above H_{c2} in Figs. 2(a)–2(d)], the following parameters were obtained: the demagnetization factors $N_x = N_y = 0.0012$ and $N_z = 0.9976$ and the internal susceptibility $\chi_{\mathrm{con}}^{\mathrm{int}} = 1.7$. This value for $\chi_{\mathrm{con}}^{\mathrm{int}} = \mu_0 M_s^2/(2AQ^2)$, where M_s is the saturation magnetization, Q is the pitch vector, and A is the stiffness, is consistent with the value of 1.76 reported in Ref. [10].

The conical phase, which exists below H_{c2}, has a more complex dynamic behavior with two modes, $+Q$ and $-Q$, corresponding to the two vibrational modes within the chiral spin texture [1,7]. The conical modulation period in Cu_2OSeO_3 is between 50 and ∼60 nm [36,37]. Both modes show a decrease in frequency with increasing field and are separated by a difference in frequency. At low field, the lower frequency $-Q$ mode contributes to a large rf absorption. With increasing field, the $-Q$ mode decreases in intensity, and the $+Q$ mode becomes the dominant mode, in agreement with the theoretically calculated behavior [10]. At H_{c2}, the $+Q$ mode continuously transforms into the field-polarized Kittel mode [7,8,10]. The dashed black lines in Figs. 2(a)–2(d) represent fits to the data using the expression given by Garst *et al.* in Eq. (30) of Ref. [10].

Further, the resonance modes have a subtle temperature dependence when traversing the field-temperature phase diagram [Figs. 2(e)–2(h)]. In the field-polarized phase, the resonance field experiences a slight increase up to $T_{\mathrm{C}} = 57$ K, above which the intensity of the mode vanishes. In the conical phase, the resonant fields of the $+Q$ and $-Q$ modes both decrease with increasing temperature at fixed frequencies.

The VNA-FMR measurements shown in Fig. 2 reveal the behavior of the resonance modes within the frequency-temperature-field phase space in Cu_2OSeO_3. However, while the presence of power-absorbing resonances is clear from these measurements, nothing can be learned about their nature. To gain further insight into their time-dependent spin structure, the dynamic contribution to the scattering at the (001) Bragg peak was measured while exciting specific ferromagnetic resonance modes.

During resonance, the precession of the magnetic moments about the equilibrium spin configuration results in a time-dependent variation of the projection of the moments along the direction of the x-ray polarization vector. This time-dependent projection in turn results in a time-dependent contribution to the scattered intensity at the (001) Bragg peak. Figure 3(a) shows a color map plot of sequences of such time-dependent scattering intensities for an excitation frequency of 4 GHz. The dynamic contributions to the scattering were recorded as a function of the time delay between the rf pump and x-ray probe pulse, and these so-called delay scans were further obtained as a function of external bias field. The yellow regions indicate that the dynamic scattering is equal to the scattered intensity from the static state, while red (blue) regions indicate an increase (decrease) in the scattered intensity. The delay scans show sinusoidal oscillations with a period of 250 ps and demonstrate that the dynamics in the spin configuration is coupled to the 4 GHz excitation frequency.

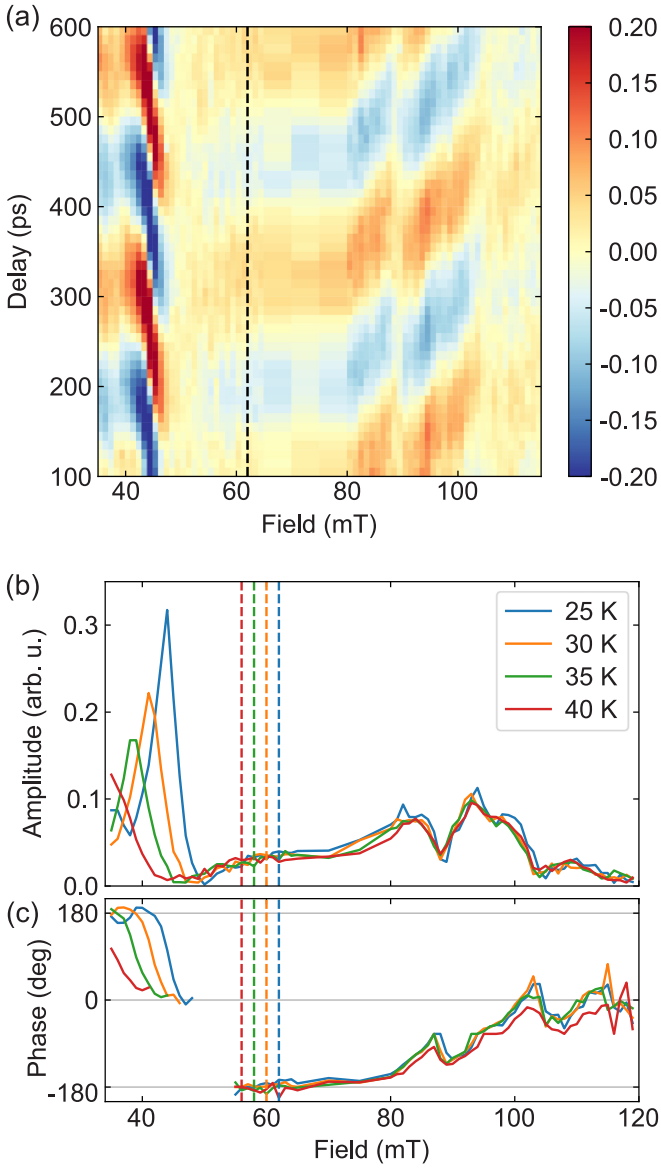

FIG. 3. (a) Color map showing the time-dependent contribution to the (001) Bragg intensity, plotted as a function of the magnetic field and the delay between the rf pump and x-ray probe. The measurements were done with an excitation frequency of 4 GHz at a temperature of 25 K with the field applied in plane and with right circularly polarized x rays at the Cu L_3 edge. The color scale represents the value of the time-dependent contribution to the (001) Bragg peak signal (in arbitrary units). (b) and (c) The amplitude and phase data extracted from sinusoidal fits to the delay scans as a function of field, respectively. The vertical lines indicate H_{c2} for the respective temperature, separating the conical and field-polarized magnetic phases.

From the contrast in Fig. 3(a) it can be seen that the amplitude and the phase of the oscillations of the (001) Bragg peak intensity change as a function of the applied magnetic field. A strong enhancement of the contrast is observed at 44 mT, and a comparably weaker enhancement is observed between 80 and 100 mT, corresponding to the two resonance modes in the 4 GHz VNA-FMR measurements at 25 K, shown in Fig. 2(a). From the shifts of the patterns across Fig. 3(a), especially around the fields at which the contrast is strong, it can also be concluded that the phase of the sinusoidal dynamic signal strongly depends on the applied magnetic field.

The dynamic contribution to the (001) Bragg intensity shown in Fig. 3(a) can be quantified via sinusoidal fits to the delay scan data at each field point. Figures 3(b) and 3(c) show the corresponding amplitude and phase, respectively, as a function of the magnetic field at 25, 30, 35, and 40 K. For all four temperatures, a peak is visible in the amplitude at ∼40 mT, corresponding to the resonance mode in the conical phase. These peaks are accompanied by a -180° phase change across the resonance. Both the magnitude and position of the amplitude peaks are a function of temperature, with the amplitude and resonant field being largest at low temperature and decreasing with increasing temperature. Both of these features are consistent with the VNA-FMR measurement data presented in Figs. 2(a)–2(d).

The amplitude [Fig. 3(b)] also shows features in the field range from 80 to 100 mT, consisting of a more complex peak structure, which is also accompanied by a (positive) phase change of 180° [Fig. 3(c)]. These features correspond to the resonance of the field-polarized phase, and they show, in contrast to the conical mode, no apparent dependence on temperature in either peak amplitude or resonance field. This behavior is consistent with the flatness of the resonance over this temperature range, which can be seen in Fig. 2(h).

Note that the $+180^\circ$ phase shift over the field-polarized resonance with field is opposite to the -180° phase shift over the conical resonance. This leading or lagging behavior of the phase is due to the different ways in which the resonance is crossed, i.e., with a negative frequency-field slope in the case of the conical resonance and a positive slope in case of the field-polarized resonance [see Fig. 2(a) for comparison]. Note that the results shown in Fig. 3 are measured with right circularly polarized light with the field applied in plane in the same orientation. When the field direction is reversed, the dynamic signal still shows a peak in amplitude for the conical resonance, and the associated 180° phase change still occurs in the same direction.

The field-polarized resonance is rather broad and shows a detailed fine structure in both amplitude and phase (Fig. 3). This behavior is due to the existence of multiple magnetostatic modes in the sample, which are enhanced due to the thin thickness of the sample [38]. These multiple overlapping resonance modes combine, resulting in the complex feature in which the higher frequency-field component is the strongest contribution. In the conical phase, these magnetostatic modes are also present but occur over a narrower frequency range and are not resolved. Note that these modes are also present in VNA-FMR measurements in both the field-polarized and conical phases but are hard to discern in the usual representation of VNA-FMR absorption maps (they become visible upon differentiation of the signal). Further, the low-field tail of the field-polarized resonance mode appears to "leak" into a field range below the H_{c2} transition, i.e., into the conical phase range. The temperature-dependent H_{c2} values are indicated by the vertical dashed lines in Figs. 3(b) and 3(c). This behavior points towards the existence of metastable states, resulting from the field-cooling protocol employed in our measurements.

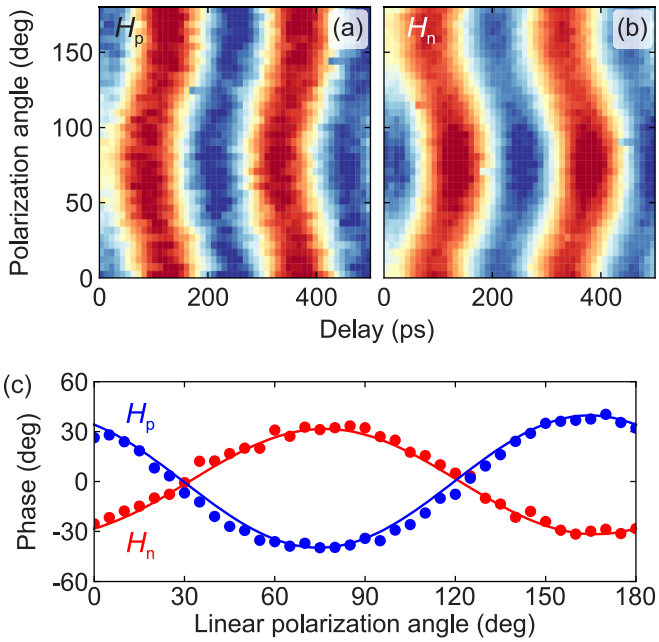

FIG. 4. Dynamic contribution to the (001) Bragg peak of the conical phase of Cu_2OSeO_3 measured at the Cu L_3 edge with linearly polarized light as a function of the linear polarization angle and the delay between rf excitation and x-ray probe pulse. The applied field was oriented in plane and (a) parallel (H_p) and (b) antiparallel (H_n) to the projection of the incident beam onto the sample plane. The sample was excited with rf at 4 GHz in an applied field of 43 mT at 25 K, i.e., exciting the conical $+Q$ resonance. (c) Phase of the dynamic contribution to the (001) Bragg peak intensity as a function of the linear polarization angle.

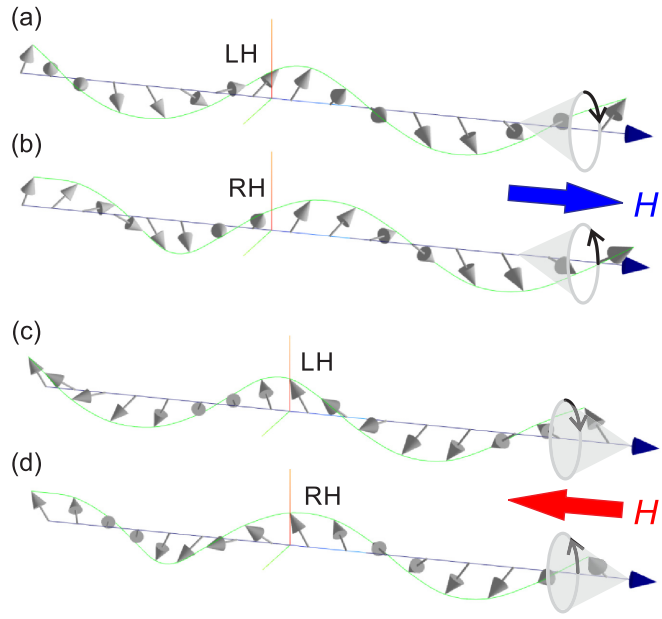

FIG. 5. Illustration of equilibrium conical spin structures for applied fields (a) and (b) along the helical propagation axis and (c) and (d) opposite to it. The sign of the Dzyaloshinskii-Moriya interaction (DMI), which is specific to the two enantiomers, results in (a) and (c) left-handed (LH) and (b) and (d) right-handed (RH) conical screws. See the Supplemental Material for a closer look at the LH conical screw in a positive applied field shown in (a) [39].

The VNA-FMR and XFMR measurements (with circularly polarized x rays) allow us to identify the resonance conditions and also obtain insight into the phase changes taking place over those resonances. However, further insight into the time evolution of the magnetic structure can be obtained by measuring the (001) Bragg diffraction of linearly polarized x rays as a function of the linear polarization angle. The linearly polarized light introduces a mechanism to provide directional contrast into the measurements of the magnetic configuration of the system.

We showed earlier that the $+Q$ resonance mode in the conical phase in our Cu_2OSeO_3 sample occurs at 4 GHz in an in-plane bias field of 43 mT at 25 K. With the system excited at this resonance, Figs. 4(a) and 4(b) show how the magnetic contrast during this dynamic process varies as a function of both the linear polarization angle and the time delay.

Similar to the measurements as a function of field in Fig. 3, the dynamic signal has a sinusoidal dependence on the delay with a period of 250 ps, originating from the 4 GHz rf excitation frequency. This dynamic signal shifts in phase as a function of the incident linear polarization angle. The particular phase of $\sim 30^\circ$ that is measured for a linear polarization angle of 0° is given by the probed position within the resonance curve at 43 mT [see Figs. 3(b) and 3(c) for comparison]. Further, the reversal of the applied field direction reverses the direction of the phase shift as a function of the incident linear polarization angle, as shown in Figs. 4(a) and 4(b) for the projection of the field along the beam direction applied parallel and antiparallel, respectively. Sinusoidal fits to the delay scan data were used to extract the phase of the dynamic signal for both positive (H_p) and negative (H_n) field, as shown in Fig. 4(c). The phase of the dynamic signals in Fig. 4(c) varies sinusoidally with the linear polarization angle. Most importantly, the phase is inverted when the direction of the magnetic field is reversed. This phase inversion can be interpreted as an inversion of the polarization angle-dependent contrast, which in resonant scattering probes the contribution of the spins along and perpendicular to the polarization direction.

In general, when the field direction is reversed and assuming that the spins simply follow the applied field, the conical spins change their equilibrium orientation, as illustrated in Fig. 5. Note that while the spins follow the magnetic field direction, the conical helix will remain either right and left handed, independent of the field direction. As the rotation sense of the dynamical precession is determined by the direction of the applied field, which is counterclockwise for a free electron spin, the rotation sense reverses (in the reference frame of the sample) if the field direction is reversed. As stated above, the conical dynamic mode which has the same (counterclockwise) rotation sense as a free spin, and therefore the field-polarized mode, is the $+Q$ mode. Both modes are seamlessly connected at the transition field H_{c2} [see Figs. 2(a)–2(d)]. Note that this behavior, i.e., the helicity of the modes, is unaffected by the chirality of the crystal [10].

In our experiments, we selected the $+Q$ mode via the rf frequency at a given applied field. Figure 6 shows an illustration

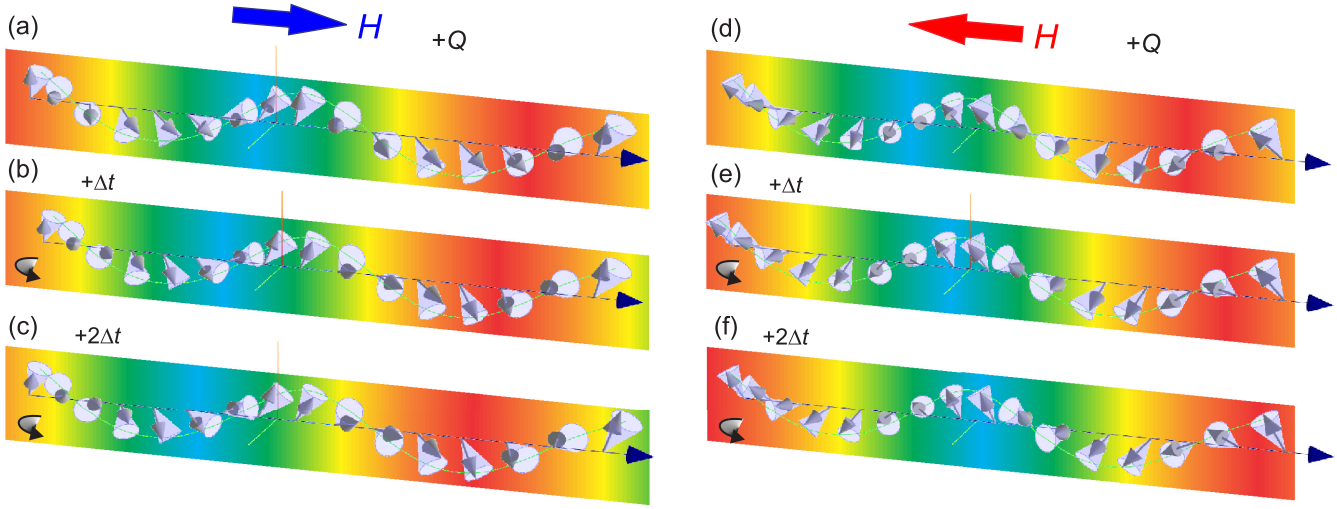

FIG. 6. Illustration of the dynamic conical spin structures (for $+Q$) in applied fields (a)–(c) along the helical propagation axis and (d)–(f) opposite to it. The panels show sequential snapshots at $t = 0$, Δt, and $2\Delta t$. The spins precess about the local effective field, describing a cone. The axes of the cones coincide with the directions of the spins in the equilibrium conical structures (green lines) shown in Fig. 5. A color scale has been superimposed as the background to indicate a compression wave where spins point closer (red) and further apart (blue) from one another. This compression wave propagates as a function of time. The propagation of the compression wave is in opposite directions upon inversion of the applied field. See the Supplemental Material for videos of both dynamical scenarios [39].

of the dynamic behavior of the $+Q$ mode upon field reversal. The panels show subsequent snapshots of the precession of the spins about the local effective field. For a positive applied field (along the helical propagation axis), a compression wave propagates to the right, in the direction of the applied field. For a negative applied field, the propagation direction inverts as well. This model is consistent with our experimental results (Fig. 4).

IV. CONCLUSIONS

In summary, we explored the dynamic phase space of the resonance modes in the conical and field-polarized states in Cu_2OSeO_3 as a function of field, temperature, and rf excitation frequency. First, we identified the resonances and measured their field and temperature dependence using VNA-FMR. Taking into account the shape (and demagnetization factors) of the Cu_2OSeO_3 sample [7], the observed modes could be reproduced using the established models [10]. Employing the same setup, synchrotron-based DFMR allowed for deeper insight into the dynamics of the identified resonance modes. We observed an inversion of the phase of the dynamic signal at 4 GHz across the resonances in the field-polarized and conical state, owing to the way the resonances are traversed. Furthermore, linearly polarized incident x rays provide additional contrast, projecting out the specific orientation of the magnetization along the incident beam propagation direction, giving access to the time-dependent orientation of the magnetic spins during precession. We found that upon reversing the applied magnetic field direction, the direction of the propagating compression wave is inverted. In general, being able to measure the time-dependent orientation of the magnetization allows for the exploration of the dynamics of chiral systems, which has so far been accessible only via rf absorption measurements in VNA-FMR. The technique of DFMR therefore provides a unique view into the magnetization dynamics of complex topologically structured spin systems.

ACKNOWLEDGMENTS

We thank Prof. M. Garst from KIT in Karlsruhe for fruitful discussion about the dynamical behavior of magnetization patterns in Cu_2OSeO_3. We acknowledge the Diamond Light Source (Oxfordshire, United Kingdom) for the provision of synchrotron radiation beam time at beamline I10 under Proposals No. SI16043 and No. SI17612. This research was funded in part by the Engineering and Physical Sciences Research Council (United Kingdom) through Grant No. EP/N032128/1.

[1] Y. Onose, Y. Okamura, S. Seki, S. Ishiwata, and Y. Tokura, Observation of Magnetic Excitations of Skyrmion Crystal in a Helimagnetic Insulator Cu_2OSeO_3, Phys. Rev. Lett. **109**, 037603 (2012).

[2] N. Nagaosa and Y. Tokura, Topological properties and dynamics of magnetic skyrmions, Nat. Nanotechnol. **8**, 899 (2013).

[3] J. F. Cochran, B. Heinrich, and A. S. Arrott, Ferromagnetic-resonance in a system composed of a ferromagnetic substrate and an exchange-coupled thin ferromagnetic overlayer, Phys. Rev. B **34**, 7788 (1986).

[4] P. J. Metaxas, R. L. Stamps, J.-P. Jamet, J. Ferre, V. Baltz, B. Rodmacq, and P. Politi, Dynamic Binding of Driven Interfaces

in Coupled Ultrathin Ferromagnetic Layers, Phys. Rev. Lett. **104**, 237206 (2010).

[5] R. Magaraggia, K. Kennewell, M. Kostylev, R. L. Stamps, M. Ali, D. Greig, B. J. Hickey, and C. H. Marrows, Exchange anisotropy pinning of a standing spin-wave mode, Phys. Rev. B **83**, 054405 (2011).

[6] A. M. Kaiser, C. Schoeppner, F. M. Roemer, C. Hassel, C. Wiemann, S. Cramm, F. Nickel, P. Grychtol, C. Tieg, J. Lindner, and C. M. Schneider, Nano and picosecond magnetization dynamics of weakly coupled CoFe/Cr/NiFe trilayers studied by a multitechnique approach, Phys. Rev. B **84**, 134406 (2011).

[7] T. Schwarze, J. Waizner, M. Garst, A. Bauer, I. Stasinopoulos, H. Berger, C. Pfleiderer, and D. Grundler, Universal helimagnon and skyrmion excitations in metallic, semiconducting and insulating chiral magnets, Nat. Mater. **14**, 478 (2015).

[8] I. Stasinopoulos, S. Weichselbaumer, A. Bauer, J. Waizner, H. Berger, M. Garst, C. Pfleiderer, and D. Grundler, Linearly polarized GHz magnetization dynamics of spin helix modes in the ferrimagnetic insulator Cu_2OSeO_3, Sci. Rep. **7**, 7037 (2017).

[9] M. Weiler, A. Aqeel, M. Mostovoy, A. Leonov, S. Geprägs, R. Gross, H. Huebl, T. T. M. Palstra, and S. T. B. Goennenwein, Helimagnon Resonances in an Intrinsic Chiral Magnonic Crystal, Phys. Rev. Lett. **119**, 237204 (2017).

[10] M. Garst, J. Waizner, and D. Grundler, Collective spin excitations of helices and magnetic skyrmions: Review and perspectives of magnonics in non-centrosymmetrric magnets, J. Phys. D **50**, 293002 (2017).

[11] S. L. Zhang, A. Bauer, H. Berger, C. Pfleiderer, G. van der Laan, and T. Hesjedal, Resonant elastic x-ray scattering from the skyrmion lattice in Cu_2OSeO_3, Phys. Rev. B **93**, 214420 (2016).

[12] S. L. Zhang, A. Bauer, D. M. Burn, P. Milde, E. Neuber, L. M. Eng, H. Berger, C. Pfleiderer, G. van der Laan, and T. Hesjedal, Multidomain skyrmion lattice state in Cu_2OSeO_3, Nano Lett. **16**, 3285 (2016).

[13] S. L. Zhang, A. Bauer, H. Berger, C. Pfleiderer, G. van der Laan, and T. Hesjedal, Imaging and manipulation of skyrmion lattice domains in Cu_2OSeO_3, Appl. Phys. Lett. **109**, 192406 (2016).

[14] S. L. Zhang, G. van der Laan, and T. Hesjedal, Direct experimental determination of the topological winding number of skyrmions in Cu_2OSeO_3, Nat. Commun. **8**, 14619 (2017).

[15] V. Ukleev, C. Luo, R. Abrudan, A. Aqeel, C. H. Back, and F. Radu, Chiral surface spin textures in Cu_2OSeO_3 unveiled by soft X-ray scattering in specular reflection geometry, Sci. Tech. Adv. Mater. **23**, 682 (2022).

[16] H. A. Dürr, E. Dudzik, S. S. Dhesi, J. B. Goedkoop, G. van der Laan, M. Belakhovsky, C. Mocuta, A. Marty, and Y. Samson, Chiral magnetic domain structures in ultrathin FePd films, Science **284**, 2166 (1999).

[17] S. L. Zhang, G. van der Laan, and T. Hesjedal, Direct experimental determination of spiral spin structures via the dichroism extinction effect in resonant elastic soft x-ray scattering, Phys. Rev. B **96**, 094401 (2017).

[18] J.-Y. Chauleau, W. Legrand, N. Reyren, D. Maccariello, S. Collin, H. Popescu, K. Bouzehouane, V. Cros, N. Jaouen, and A. Fert, Chirality in Magnetic Multilayers Probed by the Symmetry and the Amplitude of Dichroism in X-Ray Resonant Magnetic Scattering, Phys. Rev. Lett. **120**, 037202 (2018).

[19] W. Legrand, J.-Y. Chauleau, D. Maccariello, N. Reyren, S. Collin, K. Bouzehouane, N. Jaouen, V. Cros, and A. Fert, Hybrid chiral domain walls and skyrmions in magnetic multilayers, Sci. Adv. **4**, eaat0415 (2018).

[20] W. Li *et al.*, Anatomy of skyrmionic textures in magnetic multilayers, Adv. Mater. **31**, 1807683 (2019).

[21] K. T. Kim *et al.*, Chiral structures of electric polarization vectors quantified by x-ray resonant scattering, Nat. Commun. **13**, 1769 (2022).

[22] D. A. Arena, Y. Ding, E. Vescovo, S. Zohar, Y. Guan, and W. E. Bailey, A compact apparatus for studies of element and phase-resolved ferromagnetic resonance, Rev. Sci. Instrum. **80**, 083903 (2009).

[23] M. K. Marcham, P. S. Keatley, A. Neudert, R. J. Hicken, S. A. Cavill, L. R. Shelford, G. van der Laan, N. D. Telling, J. R. Childress, J. A. Katine, P. Shafer, and E. Arenholz, Phase-resolved x-ray ferromagnetic resonance measurements in fluorescence yield, J. Appl. Phys. **109**, 07D353 (2011).

[24] W. E. Bailey, C. Cheng, R. Knut, O. Karis, S. Auffret, S. Zohar, D. Keavney, P. Warnicke, J.-S. Lee, and D. A. Arena, Detection of microwave phase variation in nanometre-scale magnetic heterostructures, Nat. Commun. **4**, 2025 (2013).

[25] G. van der Laan, Time-resolved x-ray detected ferromagnetic resonance of spin currents, J. Electron. Spectrosc. Relat. Phenom. **220**, 137 (2017).

[26] A. A. Baker, A. I. Figueroa, L. J. Collins-McIntyre, G. van der Laan, and T. Hesjedal, Spin pumping in ferromagnet-topological insulator-ferromagnet heterostructures, Sci. Rep. **5**, 7907 (2015).

[27] A. A. Baker, A. I. Figueroa, D. Pingstone, V. K. Lazarov, G. van der Laan, and T. Hesjedal, Spin pumping in magnetic trilayer structures with an MgO barrier, Sci. Rep. **6**, 35582 (2016).

[28] D. M. Burn, S. Zhang, K. Zhai, Y. Chai, Y. Sun, G. van der Laan, and T. Hesjedal, Mode-resolved detection of magnetization dynamics using x-ray diffractive ferromagnetic resonance, Nano Lett. **20**, 345 (2020).

[29] D. M. Burn, S. L. Zhang, G. Q. Yu, Y. Guang, H. J. Chen, X. P. Qiu, G. van der Laan, and T. Hesjedal, Depth-Resolved Magnetization Dynamics Revealed by X-Ray Reflectometry Ferromagnetic Resonance, Phys. Rev. Lett. **125**, 137201 (2020).

[30] S. Pöllath, A. Aqeel, A. Bauer, C. Luo, H. Ryll, F. Radu, C. Pfleiderer, G. Woltersdorf, and C. H. Back, Ferromagnetic Resonance with Magnetic Phase Selectivity by Means of Resonant Elastic X-Ray Scattering on a Chiral Magnet, Phys. Rev. Lett. **123**, 167201 (2019).

[31] I. S. Maksymov and M. Kostylev, Broadband stripline ferromagnetic resonance spectroscopy of ferromagnetic films, multilayers and nanostructures, Phys. E (Amsterdam, Neth.) **69**, 253 (2015).

[32] D. H. Templeton and L. K. Templeton, Tetrahedral anisotropy of x-ray anomalous scattering, Phys. Rev. B **49**, 14850 (1994).

[33] V. E. Dmitrienko and V. A. Chizhikov, Weak Antiferromagnetic Ordering Induced by Dzyaloshinskii-Moriya Interaction and Pure Magnetic Reflections in MnSi-Type Crystals, Phys. Rev. Lett. **108**, 187203 (2012).

[34] G. van der Laan, Soft x-ray resonant magnetic scattering of magnetic nanostructures, C. R. Phys. **9**, 570 (2008).

[35] A. G. Gurevich and G. A. Melkov, *Magnetization Oscillations and Waves* (CRC Press, Boca Raton, FL, 1996).

[36] S. Seki, J.-H. Kim, D. S. Inosov, R. Georgii, B. Keimer, S. Ishiwata, and Y. Tokura, Formation and rotation of skyrmion crystal in the chiral-lattice insulator Cu_2OSeO_3, Phys. Rev. B **85**, 220406(R) (2012).

[37] S. Seki, X. Z. Yu, S. Ishiwata, and Y. Tokura, Observation of skyrmions in a multiferroic material, Science **336**, 198 (2012).

[38] B. E. Storey, A. O. Tooke, A. P. Cracknell, and J. A. Przystawa, The determination of the frequencies of magnetostatic modes in rectangular thin films of ferrimagnetic yttrium iron garnet, J. Phys. C **10**, 875 (1977).

[39] See Supplemental Material at http://link.aps.org/supplemental/10.1103/PhysRevB.106.174409 for an animated illustration of the LH conical screw in a positive applied field (Static_+Q_+H.mp4) and of the dynamic conical spin structures (for $+Q$) in applied fields along the helical propagation axis and opposite to it (Dynamics_+Q_+H.mp4 and Dynamics_+Q_-H.mp4, respectively).